

## Article

# Experimental Study on the Effect of Gas Adsorption and Desorption on Ultrasonic Velocity and Elastic Mechanical Parameters of Coal

Gang Xu <sup>1,\*</sup> , Jiawei Liu <sup>1</sup> , Yunlong Wang <sup>1</sup>, Hongwei Jin <sup>1</sup> and Chaofeng Wang <sup>2</sup><sup>1</sup> College of Safety Science and Engineering, Xi'an University of Science and Technology, Xi'an 710054, China<sup>2</sup> Xin'an Coal Mine, Henan Dayou Energy Co., Ltd., Luoyang 471842, China

\* Correspondence: xugang25193@xust.edu.cn

**Abstract:** The rapid and accurate identification of the physical characteristics of coal by means of ultrasonic detection is of great significance to ensure safe mining of coal and efficient development of coal seam methane. In this paper, the ultrasonic velocity testing experiments of coal during gas adsorption and desorption were carried out, utilizing a low frequency petrophysical measurement device with primary and fractured coal as the research objects. The variations in the elastic mechanical parameters and ultrasonic velocity of coal samples were analyzed to elucidate the influence mechanism that gas adsorption and desorption have on them. During gas adsorption and desorption, the longitudinal wave velocity of the primary structure coal varies from 1990 m/s to 2200 m/s, and the transverse wave velocity varies from 1075 m/s to 1160 m/s, while the longitudinal wave velocity of the fractured structure coal varies from 1540 m/s to 1950 m/s, and the transverse wave velocity varies from 800 m/s to 1000 m/s. The elastic modulus and wave velocities, in both directions of the primary structural coal, were higher than those of the fractured structural coal. In comparison to the fractured structural coal, the main structural coal had a lower Poisson's ratio. In addition, the spread of the elastic mechanical parameters and wave velocities, in both the longitudinal and transverse directions, was more pronounced in the fracture–structured coal than in the primary–structured coal. During gas adsorption and desorption, the speed of the coal's longitudinal waves increased, and then decreased, due to the combined effect of gas adsorption expansion and pore gas pressure compression matrix effect. For this experiment, the maximum longitudinal wave velocity of the coal occurred at a gas pressure of 1.5 MPa. Primary structural coal has a longitudinal wave speed of 2103 m/s, whereas fragmented structural coal has a speed of 1925 m/s. The variation in the shear wave velocity of the coal is controlled only by the gas adsorption expansion effects. The shear wave velocity increases during gas adsorption and decreases during gas desorption. With the change of gas pressure, the longitudinal wave velocity can increase by 23.34%, and the shear wave velocity can increase by 17.97%. Coal undergoes changes to both its Poisson's ratio and elastic modulus as a result of gas adsorption and desorption; these modifications are analogous to the velocity of longitudinal and shear waves, respectively.

**Keywords:** gas adsorption; gas desorption; ultrasonic velocity; elastic mechanical parameters; coal; porosity



**Citation:** Xu, G.; Liu, J.; Wang, Y.; Jin, H.; Wang, C. Experimental Study on the Effect of Gas Adsorption and Desorption on Ultrasonic Velocity and Elastic Mechanical Parameters of Coal. *Sustainability* **2022**, *14*, 15055. <https://doi.org/10.3390/su142215055>

Academic Editors: Xiangguo Kong, Dexing Li and Xiaoran Wang

Received: 13 October 2022

Accepted: 10 November 2022

Published: 14 November 2022

**Publisher's Note:** MDPI stays neutral with regard to jurisdictional claims in published maps and institutional affiliations.



**Copyright:** © 2022 by the authors. Licensee MDPI, Basel, Switzerland. This article is an open access article distributed under the terms and conditions of the Creative Commons Attribution (CC BY) license (<https://creativecommons.org/licenses/by/4.0/>).

## 1. Introduction

Coal is one of the important basic energy sources, which provides a solid guarantee for the sustainable and healthy development of society and economy [1–4]. In particular, China is characterized by a coal–based energy resource endowment, which concludes that coal will continue to be China's primary energy source for the foreseeable future [5,6]. Gas, also known as coalbed methane, is a gaseous medium that is produced with the formation of coal and exists mainly in the coal seam, in an adsorbed state. Gas is not only an energy,

but is also the largest source of disaster in coal mining. This is closely related to its degree of enrichment. The control and utilization of gas is closely related to its enrichment level, and the enrichment degree and its identification method have become one of the important technical problems to be solved in coal resources development [7,8].

The ultrasonic detection method is a geophysical exploration technique, which has the characteristics of good directionality, strong penetration, concentrated acoustic energy, long propagation distance and being difficult to attenuate, especially for anisotropic and biphasic media [9,10]. Gas primarily exists in the pores and fractures of coal seams in the adsorption state, and gas-bearing coals are both an anisotropic and biphasic media; it is therefore practical to use ultrasonic detection methods to identify the degree of gas enrichment in coal seams [11–14].

Since 1956, the year Biot first put forward his hypothesis of elastic wave propagation in saturated porous medium [15], the saturated fluid porous media model has been developed rapidly. However, the presence of solid medium coal, fluid phase gas and adsorbed phase gas in gas-bearing coals renders them more complicated than conventional saturated fluid porous media. The response characteristics of ultrasonic waves in gas-bearing coal have been studied intensively and extensively by domestic and foreign scientists through field tests, laboratory tests and theoretical analysis [16–20].

In their field test, Shengdong Liu and Qiufang Zhao [21,22] obtained a good negative linear correlation between gas content and inherent principal frequency of coal seam through an in-situ test of coal. Wenlin Liu [23] recognized that adsorption of methane could reduce the longitudinal wave velocity by 10–16%. Zhijun Wang and Shengdong Liu [24–26] concluded from field tests that both the longitudinal and shear wave velocities of seismic activity are reduced when the gas concentration of the coal is high. The coal seam quality factor  $Q$  was thought to be inversely linked to gas concentration, whereas the attenuation coefficient was found to be positively related to gas pressure. Pingsong Zhang [27] considered that gas content is logarithmically related to the attenuation coefficient of coal seam and linearly related to the quality factor through field acoustic detection tests, and concluded that coal seams with a quality factor less than 1 and an attenuation coefficient greater than 0.005 are high gas outburst seam.

In laboratory tests, Lixin Jiang [28] believed that saturation had no effect on shear waves in saturated porous media but had a significant effect on longitudinal waves. Jialin Hao [29] predicted that velocity of coal samples' longitudinal and transverse waves initially increases and then decrease with increasing gas pressure. Hongyi Yu [30] thought that the wave velocity of the nitrogen-containing gas continues to increase during the gas injection process. The elastic wave propagation law for gas-bearing coals is theoretically analyzed.

The author [31] concluded that the elastic wave velocity of the non-adsorbed phase model decreases slightly with increasing gas pressure, which is similar to the elastic wave velocity of a single-phase medium coal. The elastic wave velocity of the adsorbed phase model decreases significantly with increasing gas pressure, showing obvious characteristics of a two-phase medium. The results of existing studies indicate that there is a relationship between the degree of gas enrichment in coal seams and the wave velocity of coal. However, due to the limitations of the test environment and test conditions, although gas enrichment is thought to increase coal's wave speed, researchers have not reached a consensus on whether this is really the case or not.

Therefore, during the adsorption and desorption of gases in a laboratory setting, the ultrasonic response properties of a coal mass are experimentally investigated in great detail. The examination of coal's wave speed and elastic mechanical characteristics, in relation to gas pressure variations, will not only provide a basis for identifying the physical properties of coal by ultrasonic detection methods, but will also provide important guidance for the utilization of gas in mines and disaster prevention and control.

## 2. Materials and Methods

### 2.1. Experimental Equipment

The apparatus used in the ultrasonic detection experiments under gas adsorption and desorption conditions is a low frequency rock physical measurement device. Figure 1 displays the operating principle of the device. The device is primarily made up of a system for controlling the perimeter pressure, a system for controlling the pore pressure, a system for testing core samples, and a system for collecting data.

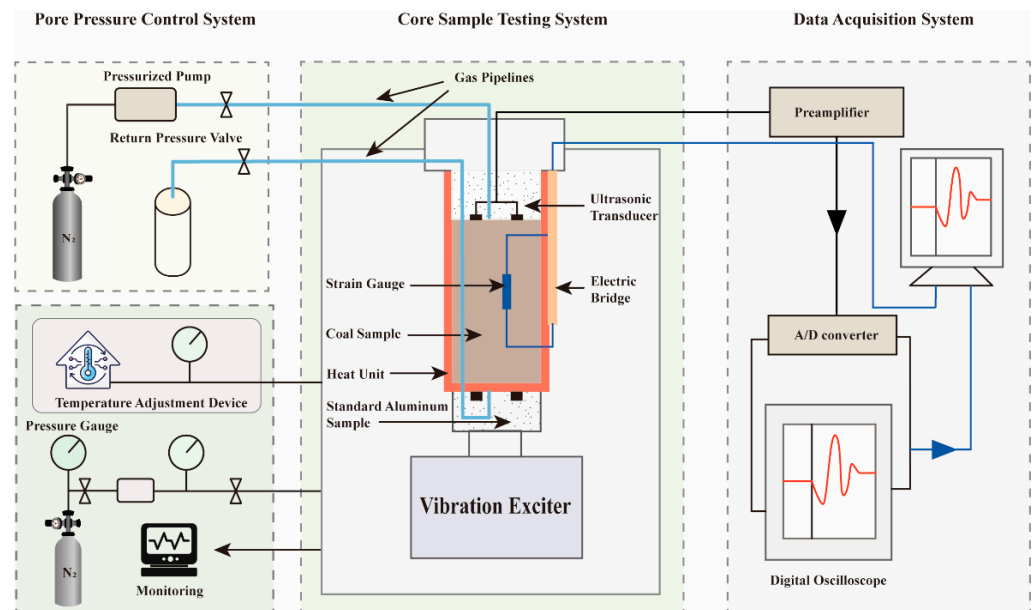


**Figure 1.** Principle of operation of the low frequency petrophysical measurement device.

#### (1) Perimeter pressure control system.

This technique used a supply of nitrogen to regulate the core sample's perimeter pressure in order to maintain the coal's pressure within a reasonable range, and the temperature adjustment device was added to the experimental system. The heating unit is controlled by the hot and cold temperature cycle regulation system in the temperature adjustment device to ensure that the experimental temperature of the coal sample is kept constant. The system was equipped with temperature and pressure monitors to allow temperature and pressure values to be read at any time. The main components included a nitrogen cylinder, booster pump, pressure indicator, pressure reducing valve, hot and cold temperature circulator, temperature indicator and heating unit.

#### (2) Pore pressure control system.

The system used a high precision pressure control pump to achieve pore pressure control and fluid displacement through a fluid rejection reactor. The high precision pressure control pump maintains a constant pressure and rate. It also allows the remote control and monitoring of pump details, including parameters such as flow rate, pressure, cylinder volume and cumulative pumping volume via flow sensors. The main components of the system are a high precision digital hydraulic pump, pressure transducer, return valve, fluid supply system and fluid displacement reactor. For this experiment, we decided to use nitrogen, rather than gas, due to safety aspects, as well as taking into consideration that coal has an equivalent adsorption effect on nitrogen to meet the experimental requirements.

#### (3) Core sample testing system.

This system is the core part of the low frequency petrophysical measurement device and is physically illustrated in Figure 2. The system allows ultrasonic measurements of coal-bearing gas to be achieved by transmitting and receiving ultrasonic waves through an ultrasonic transducer. The frequency range for ultrasonic velocity measurements is 1–5 MHz. The axial pressure measurements can be achieved by applying pressure to the

test coal sample via a servo vibrator. Pore fluid tubes can be used to achieve preheated aeration of the coal sample to simulate the variation in coal at various gas pressures. The system's essential elements include an ultrasonic transducer, servo vibrator, semiconductor strain gauge, pore fluid tube, standard aluminum sample and epoxy resin plate.



**Figure 2.** Core sample test system.

Nine layers of perforated tinfoil were chosen as the coupling agent, which solves the coupling problem without affecting the implementation of the gas injection process and effectively increases the experiment's accuracy.

#### (4) Data collection method.

The system mainly realizes high-precision data acquisition, which can record the strain and ultrasonic velocity changes of coal during the experiment. The main components of the system include control software, signal generator, 12-channel high-precision differential amplifier, servo vibration amplifier, pulse generator receiver, digital oscilloscope, digital acquisition board to place the computer and analogue digital input board.

In addition, auxiliary tools such as balances and vernier calipers are required for the experiments.

### 2.2. Principle of Measurement

The pulse transmission method is used to measure the ultrasonic velocities in low-frequency rock physics measurement systems [32,33], where ultrasonic shear wave velocities are measured primarily by picking up the first arriving shear wave using polarization cracking and then calculating its vector position. Due to the experimental conditions, the time difference between the two arrivals at the receiver decreases when the ultrasonic shear wave propagates in an anisotropic thin layer, where the fast and slow shear waves propagate in the medium in orthogonal polarization. The detector can only identify the point in time

at which the shear wave is received by the fast wave, whereas identifying the point in time at which the shear wave arrives by the slow wave is difficult. Therefore, considering the influence of practical conditions, only the speed of the shear wave is studied in this experiment.

This experiment adopted a pulse transmission ultrasonic system, and the acoustic wave velocity can be read directly by the computer. The test principle is:

$$\begin{cases} V_p = L/(t_p - t_0) \\ V_s = L/(t_s - t_0) \end{cases} \quad (1)$$

where  $V_p$  is the speed of an ultrasonic longitudinal wave (m/s),  $V_s$  is the longitudinal wave speed of ultrasound (m/s),  $L$  is the transmitting and receiving transducer spacing (m),  $t_p$  is the duration of a longitudinal wave (s),  $t_s$  is the duration of the transverse wave (s),  $t_0$  is the zero delay of the instrument system (s).

### 2.3. Coal Sample Collection and Processing

Coal samples were collected in accordance with the requirements of “Geotechnical inquiry and testing—Sampling techniques and groundwater measurements—Part 1: Technical concepts for the sampling of soil, rock, and groundwater”. They were then prepared, in accordance with international standards, into cylinders that were 50 mm in diameter and 100 mm in length [34]. The raw coal collected for the experiments was mainly primary structural coal and fractured structural coal. Considering the different orientations of the coal seam cracks, and in particular, how coal seam anisotropy affects ultrasonic transmission, care should be taken to mark the orientation, tendency and vertical lamination direction of the coal samples extracted from the coal seams when collecting them in the field.

The sampling site is in 31,004 working faces of Shanxi Xinyuan Coal Industry Co. The coal quality of this working face is medium–ash, low–sulfur, high–quality lean coal, mainly light coal, with endogenous fissures, containing 1 to 2 layers of muddy gangue, with a thickness of 0.01 to 0.04 m and an average of 0.02 m. The 3# coal seam mined at this workface is stable, with a simple structure and a solidity factor of 0.51 to 0.82. The coal sample collection requirements for this experiment were met.

Coal samples should be taken from structurally well–preserved bulk coal, placed in a pre–prepared woven bag, and marked with the type of structure and the direction in which the coal sample was collected. After collecting the primary samples, they are brought to the lab, where they are drilled into 50 mm–diameter and 100 mm–high cylindrical samples. The coal cores were ground to a flatness of less than 0.02% to allow better contact between the ultrasonic sensors and the cores.

To facilitate experimental statistics and analysis, the numbering of the coal samples was specified as follows: the direction of the parallel face cuttings was designated as the  $X$  direction; the direction of the vertical face cuttings was designated as the  $Y$  direction; and the direction of the vertical layer was designated as the  $Z$  direction (Figure 3). The drilling of this experimental coal sample was carried out in the  $X$  direction, and a total of two experimental coal samples were processed. According to the criteria for the classification of coal body structure types, primary structure coal is type I coal and fracture structure coal is type II coal. Therefore, these two coal samples can be named as IX1 and IIX1, respectively, and Table 1 displays the coal sample’s specification parameters.

**Table 1.** Statistical table of processed coal sample parameters.

Coal Sample Number	Type of Coal Structure	Length (mm)	Diameter (mm)	Fissure Development	$R_{0,max}$	$V_{daf}$ (%)	Weight Capacity ( $t \cdot m^{-3}$ )
IX1	Primary structural coal	99.9	49.9	Clearly stratified, no obvious fractures	1.86	15.7%	1.43
IIX1	Fractured structural coal	99.9	50.1	Generally clear lamination, a few fissures	1.97	16.8%	1.39

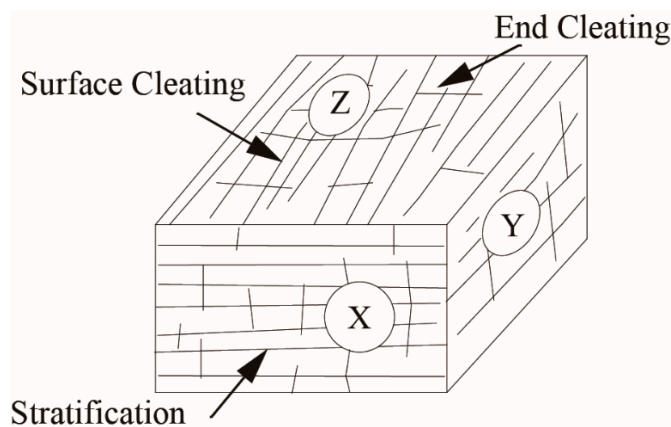


**Figure 3.** Schematic diagram of coal cuttings and laminations.

#### 2.4. Experimental Protocol and Experimental Steps

To obtain the response characteristics of the ultrasonic velocity of the coal samples during gas adsorption and desorption, the following experimental scheme was developed, according to the function of the experimental setup.

Experimental conditions: to ensure accurate experimental findings, the temperature was maintained at room temperature, approximately 25 °C, throughout the experiments. Taking into account the coal sample's low compressive strength as a whole, the axial and circumferential pressures at the beginning of the experiment were set to 3 MPa to ensure better and sufficient contact between the probe and the coal column. According to the purpose of the experiment, the experimental process was divided into three stages:

- Evacuation stage (I)
- Gas injection and adsorption stage (II)
- Pressure reduction and desorption stage (III)

Evacuation stage (I): Maintaining the axial pressure 3 MPa and the surrounding pressure 3 MPa, the coal sample was evacuated to vacuum (0.01 MPa) and the ultrasonic properties of the coal sample were tested.

Gas injection and adsorption stage (II): The technique of concurrently raising the axial pressure was used to guarantee that the coal sample's effective stress remained constant, surrounding pressure and gas pressure was used in the gas injection and adsorption stages. The coal samples were left to attain the adsorption equilibrium condition for six hours, at which point their ultrasonic properties were assessed. At this point, the injected gas pressure was 0.1 MPa, and the axial and surrounding pressures were 3.1 MPa. The ambient pressure and axial pressure were successively 3.5 MPa, 4.0 MPa, 4.5 MPa, 5.0 MPa, and 5.5 MPa when the pressure of the methane gas being injected rose to 0.5 MPa, 1.0 MPa, 1.5 MPa, 2.0 MPa, and 2.5 MPa. Subsequently, the samples were allowed to reach equilibrium by waiting for 6 h at each pressure state before testing the ultrasonic performance of the coal samples.

Desorption stage (III): The desorption stage is the antithesis of the gas injection and adsorption stages. For the desorption stage, a simultaneous reduction in shaft pressure, surrounding pressure, and gas pressure is conducted. This was achieved by reducing the shaft pressure, surrounding pressure and methane pressure in the gripper by 0.5 MPa, every 2 h, until the test was completed, at which point the methane pressure in the gripper was 0.1 MPa. The ultrasonic characteristics of the samples were tested every 2 h during the decompression process.

### 3. Results and Discussion

#### 3.1. Results from Experiments and Determination of Elastic Mechanical Characteristics

The coal sample's longitudinal wave velocity  $V_p$  and transverse wave velocity  $V_s$  during the experiments can be obtained according to the calculation method adopted by Yun Wang [35]. The dynamic–elastic mechanical parameters Poisson's ratio ( $\nu$ ) and elastic modulus ( $E$ ) may be determined from the known density  $\rho$  with  $V_p$  and  $V_s$ . Tables 2 and 3 show the findings of the evaluation of the coal sample's elastic mechanical characteristics and wave velocity.

**Table 2.** Results of tests on coal sample IX1's elastic mechanical characteristics and wave velocity.

Test No.	Shaft Pressure (MPa)	Surrounding Pressure (MPa)	Absolute Pressure (MPa)	Measurement Time (h)	Dissemination Time ( $\times 10^{-4}$ s)	Longitudinal Wave Velocity ( $m\ s^{-1}$ )	Dissemination Time ( $\times 10^{-4}$ s)	Transverse Wave Velocity ( $m\ s^{-1}$ )	Poisson's Ratio $\nu$	Elastic Modulus $E$ (GPa)
1	3.0	3.0	0.10	-	0.501	1995	0.924	1081	0.292	4.319
2	3.0	3.0	0.01	-	0.492	2031	0.914	1093	0.296	4.429
3	3.1	3.1	0.10	6	0.486	2056	0.906	1103	0.298	4.516
4	3.5	3.5	0.50	12	0.481	2075	0.900	1110	0.300	4.579
5	4.0	4.0	1.00	18	0.478	2092	0.895	1116	0.301	4.635
6	4.5	4.5	1.50	24	0.475	2103	0.891	1121	0.302	4.678
7	5.0	5.0	2.00	30	0.476	2100	0.886	1127	0.298	4.714
8	5.5	5.5	2.50	36	0.477	2095	0.883	1132	0.294	4.742
9	5.0	5.0	2.00	38	0.474	2106	0.884	1130	0.298	4.740
10	4.5	4.5	1.50	40	0.470	2125	0.888	1125	0.305	4.725
11	4.0	4.0	1.00	42	0.473	2110	0.893	1119	0.304	4.671
12	3.5	3.5	0.50	44	0.476	2098	0.896	1115	0.303	4.634
13	3.1	3.1	1.10	46	0.480	2081	0.900	1110	0.301	4.585

**Table 3.** Test results of wave velocity and elastic mechanical parameters of coal sample IIX1.

Test No.	Shaft Pressure (MPa)	Surrounding Pressure (MPa)	Absolute Pressure (MPa)	Measurement Time (h)	Dissemination Time ( $\times 10^{-4}$ s)	Longitudinal Wave Velocity ( $m\ s^{-1}$ )	Dissemination Time ( $\times 10^{-4}$ s)	Transverse Wave Velocity ( $m\ s^{-1}$ )	Poisson's Ratio $\nu$	Elastic Modulus $E$ (GPa)
1	3.0	3.0	0.10	-	0.617	1618	1.181	846	0.312	2.610
2	3.0	3.0	0.01	-	0.580	1722	1.120	892	0.317	2.912
3	3.1	3.1	0.10	6	0.559	1786	1.089	917	0.321	3.088
4	3.5	3.5	0.50	12	0.544	1836	1.066	937	0.324	3.231
5	4.0	4.0	1.00	18	0.531	1882	1.046	955	0.327	3.364
6	4.5	4.5	1.50	24	0.519	1925	1.030	970	0.330	3.478
7	5.0	5.0	2.00	30	0.522	1915	1.014	985	0.320	3.561
8	5.5	5.5	2.50	36	0.525	1902	1.001	998	0.310	3.627
9	5.0	5.0	2.00	38	0.519	1926	1.009	990	0.320	3.598
10	4.5	4.5	1.50	40	0.513	1948	1.019	980	0.331	3.553
11	4.0	4.0	1.00	42	0.523	1910	1.035	965	0.329	3.440
12	3.5	3.5	0.50	44	0.533	1873	1.050	951	0.326	3.335
13	3.1	3.1	1.10	46	0.549	1821	1.072	932	0.323	3.194

#### 3.2. Changes in the Ultrasonic Velocity of Coal Samples during Gas Adsorption and Desorption

According to Tables 2 and 3, it is possible to make the longitudinal and transverse wave velocity variation law of the coal sample during the test, as shown in Figures 4 and 5.

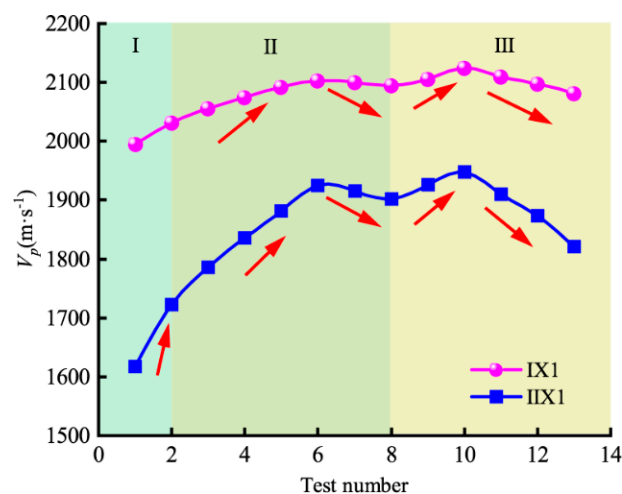


**Figure 4.** Each sample longitudinal wave velocity varies during the experiment.

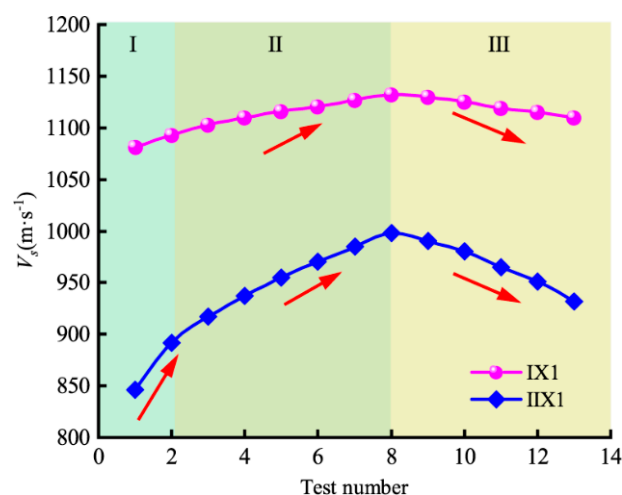


**Figure 5.** Variations in the coal sample's transverse wave velocity during the experiment.

From Figures 4 and 5, it is evident that the coal samples' longitudinal and transverse wave velocities slightly increase throughout the evacuation stage.

When the gas pressure was increased during the gas adsorption stage, from 0 MPa to 2.5 MPa, the transverse wave velocity tended to increase along with the increase in gas pressure, whereas the longitudinal wave velocity exhibited a pattern of increasing and then decreasing with the increase in gas pressure. The longitudinal wave velocity decreased as the gas pressure rose from 1.5 MPa to 2.5 MPa.

In contrast to the longitudinal wave velocity, which exhibited a pattern of growing and subsequently decreasing with the reduction in gas pressure, the transverse wave velocity showed a declining tendency, as the gas pressure dropped from 2.5 MPa to 0 MPa. The longitudinal wave velocity dropped along with the reduction in gas pressure, as it went from 1.5 MPa to 0 MPa.

Compared with the gas injection stage, the longitudinal and transverse wave velocities of the desorption stage were larger than those of the adsorption process at the same gas pressure.

In addition, the variance in the longitudinal velocity of the basic structural coal varied from 1990 m/s to 2200 m/s, as shown by Figures 4 and 5, and the variation in transverse velocity ranged from 1075 m/s to 1160 m/s, while the variation in longitudinal velocity of fractured structural coal ranged from 1540 m/s to 1950 m/s and the variation in transverse velocity ranged from 800 m/s to 1000 m/s. In all stages of the experiment, the variation in longitudinal and transverse velocities of the primary structural coal was larger than that of the fractured structural coal. At all stages of the experiment, the main structural coal has higher longitudinal and transverse wave velocities than the fractured structural coal. At all stages of the experiment, the changes of longitudinal and transverse wave velocities of the fractured structural coal were more obvious than those of the primary structural coal.

### 3.3. Changes in the Elastic Mechanical Parameters of Coal Samples during Gas Adsorption and Desorption

Based on Tables 2 and 3, the variation patterns of Poisson's ratio and the elastic modulus of the coal samples during the test period can be derived. The elastic modulus and Poisson's ratio of the coal samples both slightly rose throughout the evacuation stage, as illustrated in Figures 6 and 7. The elastic modulus exhibited an increasing trend with the increase in gas pressure in the gas adsorption stage, when the gas pressure rose from 0 MPa to 2.5 MPa, whereas the Poisson's ratio displayed a variation law of rising and then falling with the rise in gas pressure. The Poisson's ratio declined when gas pressure rose from 1.5 MPa to 2.5 MPa.

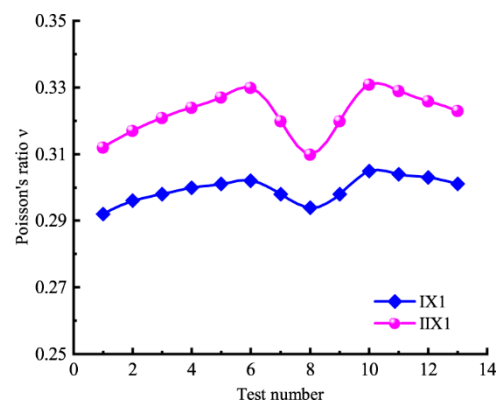


**Figure 6.** Coal sample Poisson's ratio  $\nu$  variation pattern during the course of the experiment.

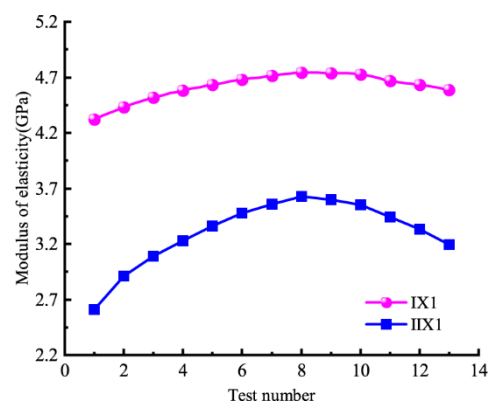


**Figure 7.** Variations in the coal sample's elastic modulus  $E$  during the course of the experiment.

The Poisson's ratio exhibited a rise and, subsequently, a reduction with the decrease in gas pressure, when the gas pressure went from 2.5 MPa to 0 MPa, but the elastic modulus showed a declining trend with the decrease in gas pressure. The Poisson's ratio rises when gas pressure falls from 1.5 MPa to 0 MPa, as seen in the graph.

Additionally, Figures 6 and 7 show that the elastic modulus  $E$  of the primary structural coal is greater than that of the fractured structural coal, whereas Figure 8 shows that the fractured structural coal's Poisson's ratio  $\nu$  is greater than that of the primary structural coal.

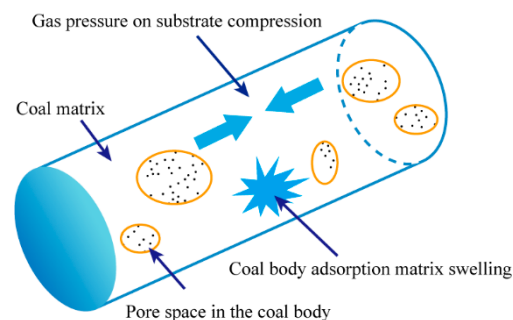


**Figure 8.** Schematic diagram of gas action inside coal body.

### 3.4. The Mechanism of How Gas Adsorption and Desorption Affect the Coal's Ultrasonic Velocity

Ultrasound is an elastic wave that is generally considered to have the greatest speed when propagating in solids and the least speed when propagating in liquids. It is generally believed that ultrasonic waves propagate with the greatest velocity in solids, followed by liquids, and the least in gases. Transverse waves can go through solids but only in liquids and gases, while longitudinal waves can move through all three.

Coal is a dual-structured pore medium consisting of matrix pores and pores [36,37]. Both free gas and adsorbed gas are present in the gas-bearing coal that results from gas adsorption; the free gas is present as a gas in the matrix pores and in the pores of the coal, while the adsorbed gas is bound to the solid surface of the coal [38]. The matrix pores, and pores of the coal that contain gas will be examined in this research to determine how gas adsorption and desorption affect coal's ultrasonic velocity when both free and adsorbed gases are present.

The following basic assumptions have been made to facilitate the study:

- The gas-bearing coal's pores and cracks were investigated, and their porosity was quantified.
- Gas containing coal underwent linear elastic minor deformation.
- It was a homogenous continuous isotropic medium that included coal.
- Gas containing coal exhibits a stress-strain relationship that abides with the generalized Hooke's law.

The deformation of coal that contains gas can be classified into two types: structural deformation and intrinsic deformation [39]. Generally, the structural deformation of gas-bearing coal is negligible because it is in the three-way ground stress field and is governed by the geological conditions of the surrounding coal seam. In addition, the experimental results in this work show that the structural deformation of the coal containing gas was constant when the axial pressure, ambient pressure, and gas pressure all increased at the same time. As illustrated in Figure 8, the ontogenetic deformation of gas-bearing coal is caused by the adsorption and desorption of gas, and the parameters influencing this deformation include gas pressure and adsorption.

The strain in the coal, due to the expansion of the adsorbed gas, is [40]:

$$\varepsilon_{BX} = \frac{2a\rho RT(1-2\nu)}{3EV_m(1-\varphi_0)} \ln(1+bp) \quad (2)$$

where  $\varepsilon_{BX}$  is the strain caused by the expansion of adsorbed gas,  $\rho$  is the apparent density of coal ( $\text{kg}/\text{m}^3$ ),  $\nu$  is the Poisson's ratio,  $E$  is the elastic modulus (MPa),  $a$  is the ultimate adsorption capacity at a given temperature ( $\text{m}^3/\text{t}$ ),  $V_m = 22.4 \times 10^{-3} \text{ m}^3/\text{mol}$ ,  $V_m$  is the molar volume of gas,  $b$  represents half of the pressure corresponding to the pressure at which the ultimate adsorption capacity is reached ( $\text{MPa}^{-1}$ ),  $R$  is the universal gas constant,  $T$  is the temperature (K),  $p$  is the gas pressure (MPa),  $R = 8.3143 \text{ J}/(\text{mol}\cdot\text{K})$ ,  $\varphi_0$  is the porosity.

Following a shift in the pore gas pressure, coal matrix compression experiences a linear strain [41]:

$$\varepsilon_{BP} = \frac{C_S}{3} p \quad (3)$$

where  $\varepsilon_{BP}$  is the linear strain, a result of the coal matrix mass's compression caused by pore gas pressure, and  $C_S$  is the coal matrix mass compression factor.

The coal's longitudinal and transverse wave velocities were computed using the following formulas, taking into account the effects of gas adsorption and gas pressure:

$$v_z = \frac{L}{\frac{L-L(1-\varphi_0)(1+\varepsilon_{BX}+\varepsilon_{BP})}{v_k} + \frac{L(1-\varphi_0)(1+\varepsilon_{BX}+\varepsilon_{BP})}{v_{zs}}} \quad (4)$$

$$v_h = v_{hs}(1-\varphi_0)(1+\varepsilon_{BX}) \quad (5)$$

where  $v_{zs}$  represents ultrasonic longitudinal velocity in the matrix (m/s),  $L$  represents length of the coal unit (m),  $v_k$  represents ultrasonic velocity in the pore gas (m/s),  $v_z$  represents ultrasonic longitudinal velocity in the coal unit (m/s),  $v_h$  represents ultrasonic transverse velocity in the coal unit (m/s),  $v_{hs}$  represents ultrasonic transverse velocity in the matrix (m/s).

As gas adsorption and desorption affect the same mechanism of wave velocity variation in primary and cracked structural coals, the ultrasonic velocity variation during gas

adsorption is analyzed below as an example for coal sample IX1, and the basic parameters of coal sample IIX1 are represented in Table 4.

**Table 4.** Coal sample IX1's elastic mechanical characteristics and gas seepage parameters.

$\rho/(\text{t}\cdot\text{m}^{-3})$	$E/\text{MPa}$	$\nu$	$a/(\text{m}^3\cdot\text{t}^{-1})$	$b/(\text{MPa}^{-1})$	$\varphi_0$	$T/\text{K}$	$C_S/(\text{MPa}^{-1})$	$V_p/(\text{m}\cdot\text{s}^{-1})$	$V_s/(\text{m}\cdot\text{s}^{-1})$
1.43	4400	0.296	35.2	0.71	0.06	298	0.016	2031	1093

The calculation regarding the speed of propagation of sound waves in gas gases is based on the equation [42]:

$$v_k = \sqrt{\frac{rRT}{M}} \quad (6)$$

where  $r$  is the proportion of a gas's constant–pressure heat capacity to its constant–temperature heat capacity, for methane 1.33,  $M$  is the gas's molecular weight, for methane  $16 \times 10^{-3}$  ( $\text{kg}\cdot\text{mol}^{-1}$ ), and  $T$  is the absolute temperature (K).

According to Equation (6), the ultrasonic velocity in the gas  $v_k = 453.94$  m/s. According to Equations (4) and (5), simultaneously, the coal matrix velocity  $v_{zs} = 2607.9$  m/s and  $v_{hs} = 1162.8$  m/s.

By substituting the combination of Equations (4) and (5) into the elastic dynamics and gas percolation parameters of different coal samples, the calculated values of the longitudinal and transverse wave velocities of coal containing gas at different test stages could be obtained, and the comparison between the experimental values is shown in Figures 9 and 10.

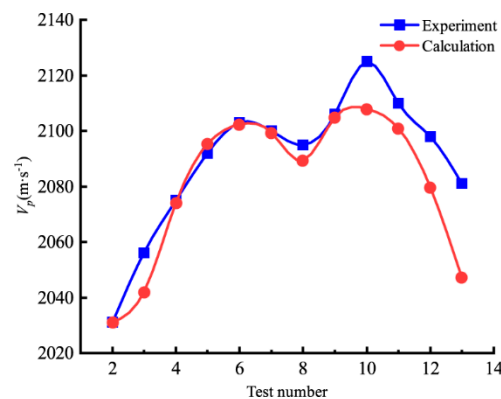


**Figure 9.** Variation of calculated and experimental values of longitudinal wave velocity of coal sample during the experiment.

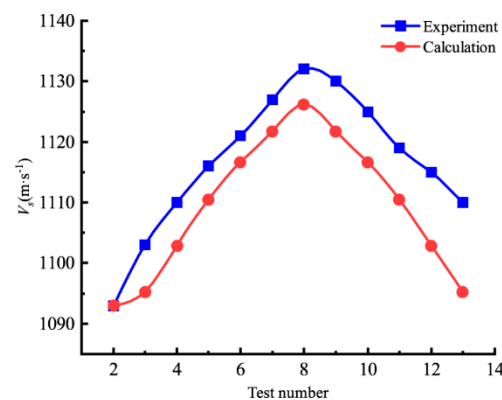


**Figure 10.** Variation of calculated and experimental values of transverse wave velocity of coal sample during the experiment.

Figures 9 and 10 show that there is a general agreement between the estimated and experimental values for the coal's longitudinal and transverse wave velocities during gas adsorption and desorption, as well as for their magnitudes.

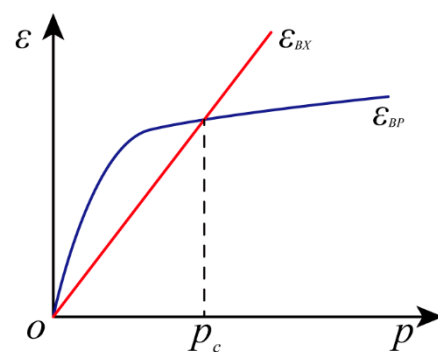
There is a crucial gas pressure value (1.5 MPa) that produces the greatest longitudinal wave velocity of coal during the jet adsorption stage, where the longitudinal wave velocity of coal exhibits a trend of growing and subsequently dropping. As the gas pressure rises during the jet adsorption step, the coal's transverse wave velocity also rises. The coal's longitudinal wave velocity, similarly, has a tendency to rise and then fall throughout the stage of decreasing desorption. The greatest longitudinal wave velocity of coal is caused by a critical gas pressure of 1.5 MPa. The coal's transverse wave velocity drops when the gas pressure drops during the downward desorption stage.

Additionally, during the descending desorption stage, the longitudinal wave velocity of coal, measured experimentally, is a little bit higher than the longitudinal wave velocity estimated. The coal's longitudinal wave velocity in the descending desorption stage was higher, under the same gas pressure circumstances, than it was in the gas injection and adsorption phases.

The above results indicate that it is feasible to analyze the variation in longitudinal and transverse wave velocities of coal during gas adsorption and desorption by using factors such as the adsorption and expansion of gas on the coal matrix and the compression of the coal matrix by pore gas pressure. The mechanism of coal's longitudinal and transverse wave velocity fluctuation will be further explained in the section that follows, from the viewpoint of how coal's porosity is affected by gas adsorption and desorption.

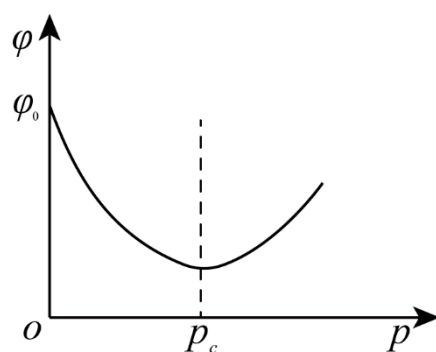
The results show that the porosity of coal is the main factor affecting the longitudinal wave velocity of coal, which will change during gas adsorption and desorption due to the influence of gas adsorption and desorption, resulting in the coal's longitudinal wave velocity changing.

Figure 11 shows the variation of strain in coal with gas pressure. The compression substrate is subjected to equal-sized stresses. The gas adsorption expansion strain was larger than the strain on the gas compression substrate when the gas pressure was less than the critical gas pressure  $p_c$ , and vice versa when the gas pressure was higher than the critical gas pressure  $p_c$ .



**Figure 11.** Variation of strain in coal with gas pressure.

Figure 12 shows the variation in the porosity of the coal with gas pressure, and combining Figures 11 and 12, it is clear that the coal's porosity suffered as a result of the gas adsorption expansion strain, whereas the gas compression matrix strain exhibited a positive effect on the porosity of coal. When the gas pressure dropped below the critical gas pressure  $p_c$ , the gas adsorption expansion strain was greater than the gas compression matrix strain, thus showing a continuous decrease in coal porosity. When the gas pressure dropped below the critical gas pressure  $p_c$ , the gas adsorption expansion strain was less than the gas compression matrix strain, thus showing a continuous increase in coal porosity. Therefore, as gas pressure rises, coal porosity exhibits a pattern of falling and then rising.



**Figure 12.** Variation of porosity in coal with gas pressure.

It is generally believed that there is a negative correlation between the coal's porosity and longitudinal velocities. Whenever there is a drop in gas pressure, to below the critical gas pressure (1.5 MPa), the negative effect of gas adsorption and expansion strain is greater than the positive effect of the gas compression matrix strain, and the porosity of coal de-crumple, leading to an increase in the longitudinal velocity of coal. Additionally, if the gas pressure exceeds the critical gas pressure (1.5 MPa), the negative effect of gas adsorption and the expansion strain is smaller than the positive effect of the gas compression matrix strain, and the porosity of the coal increases, leading to the decrease in the longitudinal velocity of the coal. If the gas pressure is higher than the critical gas pressure (1.5 MPa), the negative effect of the gas adsorption expansion strain is smaller than the positive effect of the gas compression matrix, at which point the porosity of the coal body increases, leading to a reduction in the coal body's longitudinal velocity. In the decompression desorption stage, the positive effect of the gas compression matrix strain decreases more significantly as the gas pressure decreases, if the gas pressure is higher than the critical gas pressure (1.5 MPa), at which point the porosity of the coal body decreases, leading to an increase in the longitudinal velocity of the coal body.

The negative impact of the gas adsorption expansion strain is lessened when the gas pressure is below the critical gas pressure (1.5 MPa). At this point, the coal body's porosity rises, increasing the coal body's longitudinal velocity. The negative effects of the gas adsorption expansion strain become less pronounced, and the coal body's porosity rises when the gas pressure is below the critical gas pressure (1.5 MPa), which results in a drop in the longitudinal wave velocity.

The transverse wave can only travel through solids; therefore, the impact of gas adsorption and expansion is the sole factor affecting the transverse wave velocity of coal bodies. The coal body's adsorption and expansion strain rise with the gas pressure, increasing the transverse wave velocity. The coal body's adsorption and expansion strain reduce with a fall in gas pressure, and as a result, so does the transverse wave velocity. The coal body's transverse wave velocity is highest when the gas pressure is 2.5 MPa.

### *3.5. Mechanisms through Which Variations in the Elastic Mechanical Properties of Coal Masses Are Influenced by Gas Adsorption and Desorption*

The elastic mechanical parameters of the coal body are an external reflection of the physical properties of the coal body. Research shows that gas adsorption and desorption can affect the mechanical properties of a coal body. Moreover, gas adsorption and desorption are the result of the combined effect of gas adsorption expansion and gas compression matrix effect. Therefore, gas adsorption expansion and gas compression matrix effect are the root causes of the changes to the elastic mechanical parameters of coal body during gas adsorption and desorption.

During gas injection, if the gas pressure is below the critical gas pressure (1.5 MPa), the gas adsorption expansion effect of the coal skeleton is greater than the gas compression matrix effect, and the overall coal body shows rheological characteristics due to the gas adsorption expansion, and therefore, the Poisson's ratio increases. The critical gas pressure

is exceeded when the gas pressure is high, the gas compression matrix effect dominates, and the overall coal body shows hardening due to the gas compression matrix effect. The critical gas pressure is exceeded when the gas pressure is high, the gas compression matrix effect is dominant, and the overall coal body shows hardening due to the gas compression matrix effect. In the desorption process, the critical gas pressure is exceeded when the gas pressure is high, the gas compression matrix effect decreases more blatantly, and the Poisson's ratio increases again. If the gas pressure drops more and falls below the critical gas pressure (1.5 MPa), the gas adsorption expansion effect drops more blatantly, so the Poisson's ratio diminishes again. Meanwhile, the theoretical formula of Poisson's ratio is accurately represented by  $\nu = \left( V_p^2 - 2V_s^2 \right) / \left[ 2 \left( V_p^2 - V_s^2 \right) \right]$ . Poisson's ratio is positively correlated with the longitudinal and transverse wave velocity ratios. The longer the ratio of longitudinal to transverse wave speed, the bigger the Poisson's ratio, which is inversely proportional to the ratio of wave speed. The same variation rule applies to both the Poisson's ratio and the longitudinal wave speed.

A measurement of an object's resistance to elastic deformation is its elastic modulus. The expansion rate of the coal skeleton during the process of gas adsorption rises with an increase in gas pressure, which is represented as a rise in the elastic modulus of the coal body. As the gas pressure drops during the pressure desorption process, the coal skeleton's rate of gas adsorption expands less quickly, which is stated as a reduction in the elastic modulus of the coal body. Meanwhile, the theoretical equation of elastic modulus can also illustrate the above conclusion. From  $\mu = \rho V_s^2$ , it is known that the larger the transverse wave velocity is, the larger the shear modulus of the coal sample is; subsequently, according to  $E = 2\mu(1 + \nu)$ , the elastic modulus is positively related to the shear modulus, so the elastic modulus is in line with the trend of the transverse wave velocity.

#### 4. Conclusions

(1) During the gas adsorption and desorption processes, the longitudinal and transverse wave velocities of the primary structural coal are greater than those of the fractured structural coal, and the change amplitude of the longitudinal and transverse wave velocities of the fractured structural coal is more noticeable than that of the primary structural coal.

(2) The coal body's longitudinal wave velocity can only increase beyond a critical gas pressure threshold, which in this experiment is 1.5 MPa. As a result of the gas adsorption and desorption processes, the coal's longitudinal wave velocity initially rises and subsequently falls. The transverse wave velocity and gas pressure have a strong positive association.

(3) The combined effects of the gas adsorption expansion effect and the gas compression matrix impact result in the change in the longitudinal wave velocity of the coal body.

(4) The change in the transverse wave velocity is compatible with the changing law of gas pressure. The variation in the transverse wave velocity of coal is exclusively regulated by the gas adsorption expansion effect.

(5) During the gas adsorption and desorption process, the coal's elastic modulus and Poisson's ratio both change at the same rates as the longitudinal and transverse wave velocities.

**Author Contributions:** Conceptualization, G.X.; methodology, G.X.; validation, G.X., C.W. and J.L.; formal analysis, J.L. and Y.W.; investigation, Y.W.; writing—original draft preparation, G.X. and Y.W.; writing—review and editing, G.X. and J.L.; visualization, J.L.; supervision, H.J.; project administration, G.X.; funding acquisition, G.X. All authors have read and agreed to the published version of the manuscript.

**Funding:** This research was funded by the National Key Research and Development Program of China, No. 2018YFC0807805; the Natural Science Basic Research Program of Shaanxi, No. 2019JM-072.

**Institutional Review Board Statement:** Not applicable.

**Informed Consent Statement:** Not applicable.

**Data Availability Statement:** Not applicable.

**Acknowledgments:** We appreciate all of the writers' assistance and efforts in helping to write this article.

**Conflicts of Interest:** The authors state that they have no conflict of interests.

## References

1. Liu, P.; Liu, A.; Zhong, F.; Jiang, Y.; Li, J. Pore/fracture structure and gas permeability alterations induced by ultrasound treatment in coal and its application to enhanced coalbed methane recovery. *J. Pet. Sci. Eng.* **2021**, *205*, 108862. [[CrossRef](#)]
2. Wang, X.; Wang, E.; Liu, X.; Zhou, X. Failure mechanism of fractured rock and associated acoustic behaviors under different loading rates. *Eng. Fract. Mech.* **2021**, *247*, 107674. [[CrossRef](#)]
3. Kong, X.; He, D.; Liu, X.; Wang, E.; Li, S.; Liu, T.; Ji, P.; Deng, D.; Yang, S. Strain characteristics and energy dissipation laws of gas-bearing coal during impact fracture process. *Energy* **2022**, *242*, 123028. [[CrossRef](#)]
4. Liu, X.; Jia, T.; Wei, J.; Wei, G.; Yan, J.; Wu, C. Modeling and evolution characteristics of coal reservoir energy during gas and water production. *J. Nat. Gas Sci. Eng.* **2021**, *96*, 104329. [[CrossRef](#)]
5. Zhou, A.; Du, C.A.; Wang, K.; Hu, J.; Fan, X. Experimental research on the law of the deformation and damage characteristics of raw coal/briquette adsorption-instantaneous pressure relief. *Fuel* **2022**, *308*, 122062. [[CrossRef](#)]
6. Yuan, L. Strategies of high efficiency recovery and energy saving for coal resources in China. *J. Southwest Pet. Univ. Sci. Technol. Ed.* **2018**, *20*, 3–12. [[CrossRef](#)]
7. Liu, X.; Zhang, F.; Ma, G.; Su, X. Analysis and applied study on key factors of coal and rock crack network reconstruction. *Coal Sci. Technol.* **2017**, *45*, 85–89+169. [[CrossRef](#)]
8. Wang, X.; Asem, P.; Hu, C.; Labuz, J.F. Microcracking in tensile fracture of a brittle rock. *Eng. Fract. Mech.* **2021**, *251*, 107789. [[CrossRef](#)]
9. Cheng, L.; Wang, Y.; Zhang, Y.; Zhao, H. The present situation and prospect of the acoustic properties research in coal. *Prog. Geophys.* **2013**, *28*, 452–461. [[CrossRef](#)]
10. Shen, X.; Xiong, Q.; Shi, W.; Liang, S.; Shi, X.; Wang, K. A New Algorithm for Reconstructing Two-Dimensional Temperature Distribution by Ultrasonic Thermometry. *Math. Probl. Eng.* **2015**, *2015*, 916741. [[CrossRef](#)]
11. Karacan, C.Ö. Swelling-induced volumetric strains internal to a stressed coal associated with CO<sub>2</sub> sorption. *Int. J. Coal Geol.* **2007**, *72*, 209–220. [[CrossRef](#)]
12. Li, H.; Lin, B.; Yang, W.; Zheng, C.; Hong, Y.; Gao, Y.; Liu, T.; Wu, S. Experimental study on the petrophysical variation of different rank coals with microwave treatment. *Int. J. Coal Geol.* **2016**, *154–155*, 82–91. [[CrossRef](#)]
13. Liu, P.; Fan, L.; Fan, J.; Zhong, F. Effect of water content on the induced alteration of pore morphology and gas sorption/diffusion kinetics in coal with ultrasound treatment. *Fuel* **2021**, *306*, 121752. [[CrossRef](#)]
14. Wang, L.L.; Vandamme, M.; Pereira, J.M.; Dangla, P.; Espinoza, N. Permeability changes in coal seams: The role of anisotropy. *Int. J. Coal Geol.* **2018**, *199*, 52–64. [[CrossRef](#)]
15. Biot, M.A. Theory of propagation of elastic waves in a fluid-saturated porous solid. I. Low-frequency range. *J. Acoust. Soc. Am.* **1956**, *28*, 168–178. [[CrossRef](#)]
16. Busch, A.; Gensterblum, Y.; Krooss, B.M.; Siemons, N. Investigation of high-pressure selective adsorption/desorption behaviour of CO<sub>2</sub> and CH<sub>4</sub> on coals: An experimental study. *Int. J. Coal Geol.* **2006**, *66*, 53–68. [[CrossRef](#)]
17. Liu, P.; Qin, Y.; Liu, S.; Hao, Y. Non-linear gas desorption and transport behavior in coal matrix: Experiments and numerical modeling. *Fuel* **2018**, *214*, 1–13. [[CrossRef](#)]
18. Mao, Y.; Chen, Y.; Bu, X.; Xie, G. Effects of 20 kHz ultrasound on coal flotation: The roles of cavitation and acoustic radiation force. *Fuel* **2019**, *256*, 115938. [[CrossRef](#)]
19. Pan, Z.; Connell, L.D. A theoretical model for gas adsorption-induced coal swelling. *Int. J. Coal Geol.* **2007**, *69*, 243–252. [[CrossRef](#)]
20. Wang, G.X.; Wei, X.R.; Wang, K.; Massarotto, P.; Rudolph, V. Sorption-induced swelling/shrinkage and permeability of coal under stressed adsorption/desorption conditions. *Int. J. Coal Geol.* **2010**, *83*, 46–54. [[CrossRef](#)]
21. Liu, S.; Zhao, Q.; Zhang, P.; Guo, L. Test and research on relationship between seam gas features and vibration wave parameters. *Coal Sci. Technol.* **2005**, *33*, 33–36. [[CrossRef](#)]
22. Zhao, Q.; Hou, Y.; Liu, S. The pilot study on characteristics of the seismic wave spectrum and gas content of coal seam. *J. Henan Polytech. Univ.* **2008**, *27*, 615–618. [[CrossRef](#)]
23. Liu, W. Geophysical response characteristics of coalbed methane. *Lithol. Reserv.* **2009**, *21*, 113–115. [[CrossRef](#)]
24. Liu, S.; Zhao, Q.; Zhang, P.; Guo, L. Study on Gas Content and the Attenuation Characteristics of Coal Seams of Huainan Xinzhuangzi Mine. *J. Anhui Univ. Sci. Technol. Nat. Sci.* **2005**, *25*, 1–4. [[CrossRef](#)]
25. Wang, Z.; Liu, S.; Lu, T.; Zhang, P.; Zhao, L. Experimental study on the relationships of coal gas and seismic attributes. *Coal Geol. Explor.* **2011**, *39*, 63–65. [[CrossRef](#)]
26. Wang, Z.; Liu, S.; Zhang, X. Correlation analysis of apparent seismic wave speeds and gas parameters in front of the coal roadway. *Prog. Geophys.* **2012**, *27*, 349–354. [[CrossRef](#)]
27. Zhang, P.; Liu, S.; Qiufang, Z.; Guo, L. Factor analysis on seam reduced features and quality in Huainan Mining Area. *Coal Sci. Technol.* **2006**, *34*, 83–85. [[CrossRef](#)]

28. Jiang, L.; Shi, X. Relation between wave velocity in sandstone and fluid content in porous medium under high frequency condition. *Oil Geophys. Prospect.* **1998**, *33*, 355–362. [[CrossRef](#)]
29. Hao, J. Experimental research on ultrasonic elastic characteristics of outburst coal. Master's Thesis, China University of Mining and Technology, Xuzhou, China, 2019.
30. Yu, H. Ultrasonographic Features and Mechanism of Anisotropic about the Coal Containing Nitrogen (Water). Master's Thesis, Henan Polytechnic University, Jiaozuo, China, 2016.
31. Xu, G.; Deng, X.; Zhang, K.; Liu, W. Research on propagation law of waves in coal seam containing gas. *Saf. Coal Mines* **2009**, *40*, 1–4. [[CrossRef](#)]
32. Xu, X. Research on the Ultrasonic Characteristics of Coal Under Normal Temperature and Pressure Conditions. Master's Thesis, Henan Polytechnic University, Jiaozuo, China, 2013.
33. Zhao, Y.; Zhang, Y.; Wang, S. Experimental Study on Ultrasonic Anisotropic Characteristics of Nitrogen-containing Coal Bodies. *J. Southwest Pet. Univ. Sci. Technol. Ed.* **2018**, *40*, 83–90. [[CrossRef](#)]
34. *Geotechnical Investigation and Testing—Sampling Methods and Groundwater Measurements—Part 1: Technical Principles for the Sampling of Soil, Rock and Groundwater*; International Organization for Standardization: Geneva, Switzerland, 2021.
35. Wang, Y.; Xu, X.; Zhang, Y. Characteristics of P-wave and S-wave velocities and their relationships with density of six metamorphic kinds of coals. *Chin. J. Geophys.* **2012**, *55*, 3754–3761. [[CrossRef](#)]
36. Law, B.E.; Rice, D.D. *Hydrocarbons from Coal*; American Association of Petroleum Geologists: Tulsa, OK, USA, 1993.
37. Kong, X.; Wang, E.; Li, S.; Lin, H.; Xiao, P.; Zhang, K. Fractals and chaos characteristics of acoustic emission energy about gas-bearing coal during loaded failure. *Fractals* **2019**, *27*, 1950072. [[CrossRef](#)]
38. Jia, L.; Yu, Y.; Li, Z.-P.; Qin, S.-N.; Guo, J.-R.; Zhang, Y.-Q.; Wang, J.-C.; Zhang, J.-C.; Fan, B.-G.; Jin, Y. Study on the Hg<sup>0</sup> removal characteristics and synergistic mechanism of iron-based modified biochar doped with multiple metals. *Bioresour. Technol.* **2021**, *332*, 125086. [[CrossRef](#)] [[PubMed](#)]
39. Lu, P.; Sheng, Z.; Zhu, G.; Fang, E. The effective stress and mechanical deformation and damage characteristics of gas-filled coal. *J. Univ. Sci. Technol. China* **2001**, *31*, 686–693. [[CrossRef](#)]
40. Wu, S.; Zhao, W. Analysis of effective stress in adsorbed methane-coal system. *Chin. J. Rock Mech. Eng.* **2005**, *24*, 1674–1678. [[CrossRef](#)]
41. Li, P.; Kong, X.; Lu, D. Mathematical modeling of flow in saturated porous media on account of fluid-structure coupling effect. *Chin. J. Hydrodyn.* **2003**, *18*, 419–426. [[CrossRef](#)]
42. Han, X.; Xu, D.; Guo, J.; Yang, L.; Wang, Z.; Zhang, D.; Luo, X.; Nie, J.; Li, H.; Jiang, J. Rock physics modelling for acoustic velocities of sandstone considering effects of cementation and compaction. *Chin. J. Geophys.* **2018**, *61*, 5044–5051. [[CrossRef](#)]